SUPPLEMENTAL MATERIAL FOR

3D 0-10 HZ PHYSICS-BASED SIMULATIONS OF THE 2020 MAGNA, UTAH EARTHQUAKE SEQUENCE

DISCONTINUOUS MESH

For all simulations in this project we use the 3D finite difference code AWP-ODC with support for discontinuous mesh (Nie et al., 2017) at the Oak Ridge Leadership Computing Facility (OLCF) using Summit GPU nodes. In order to maximize computational efficiency and to obtain sufficient resolution of the grid, we design the mesh with 3 blocks as shown in Fig. S1, which ensures at least 5 points per minimum wavelength throughout the model (minimum V_s=125 m/s).

POINT SOURCE MODEL FOR MAGNA AFTERSHOCK

We follow Brune (1970) in our definition of the point source spectrum for the M_w4.59 Magna aftershock, with the Fourier moment rate spectrum expressed as

$$\Omega(f) = \frac{M_0}{1+(f/f_c)^2} \quad , \tag{S1}$$

where M_0 is the scalar moment in $N \cdot m$, and f_c is the corner frequency determined by

$$\begin{aligned} f_c &= kV_S \left(\frac{16}{7} \cdot \frac{\Delta\sigma}{M_0} \right)^{\frac{1}{3}} \\ &= 0.49 V_S \left(\frac{\Delta\sigma}{M_0} \right)^{\frac{1}{3}} \quad , \end{aligned} \tag{S2}$$

where $k = 0.372$ is Brune's constant for S waves, V_s is the shear velocity around the point source in m/s, and $\Delta\sigma$ is the stress drop in Pa. After applying inverse Fourier transformation to Eq. (S1), the minimum-phase slip rate source time function is derived as

$$\Omega(t; f_c) \propto t \cdot \exp\left[-2\pi f_c t\right] \cdot H(t) \quad , \tag{S3}$$

where $H(t)$ is the Heaviside step function.

LOW-VELOCITY TAPER METHOD

The low-velocity taper (LVT) following Ely et al. (2010) is described as

$$\begin{aligned} z_r &= z/z_T \quad , \\ f(z_r) &= z_r + b(z_r - z_r^2) \quad , \\ g(z_r) &= a - a z_r + x \cdot (c^2 + 2\sqrt{z_r} - 3z_r) \quad , \\ V_S(z_r) &= f(z_r) \cdot V_{ST} + g(z_r) \cdot V_{S30} \quad , \end{aligned} \tag{S4}$$

where z_T and z_r are the tapering bottom depth and the depth ratio, respectively, a, b, c are three shape-controlling parameters, V_{ST} is the original V_s at z_T, and V_{S30} is the time-averaged shear velocity in the top 30 m. Since the near-surface low velocity material is already included in the WFCVM, the LVT is only applied to the areas outside the basin, where the near-surface velocities appear over-simplified in the CVM with surface V_s around 1400 m/s. Fig. S2 compares the 1D V_s profiles at the two rock stations NOQ and RBU (see Fig. 1(b) for locations) with and without the 1,000 m LVT, and Fig. S3 compares the surface V_s of the model area with and without the LVT and SSHs.

CALCULATION OF REFERENCE STRAINS

The reference strains are calculated based on an empirical relation following Darendeli (2001) as

$$\gamma_r = (\phi_1 + \phi_2 PI \cdot OCR^{\phi_3})\sigma_0^{\phi_4} \quad , \tag{S5}$$

where ϕ_{1-4} are empirical constants, PI is the modified plasticity index, and OCR is the normal consolidation factor. The resulting γ_r is in units of % when the confining pressure σ_0 is converted to the standard atmosphere unit (atm), after being derived from the vertical stress component τ_{zz} and pore pressure σ_{PP} at depth h

$$\begin{aligned} \sigma_0 &= -(\tau_{zz}) - \sigma_{PP} \\ &= \begin{cases} \int_{z=0}^{h} [\rho_{soil}(z) g] \cdot dz, & (h \le h_{gw}) \\ \int_{z=0}^{h} [\rho_{soil}(z) g] \cdot dz - \rho_{water} g \cdot (h - h_{gw}), & (h > h_{gw}) \end{cases} \quad , \end{aligned} \tag{S6}$$

where $\rho_{soil}(z)$ is the depth-dependent soil density, ρ_{water} is the density of water, and h_{gw} is the depth to the ground water level. As an average model applied to the Salt Lake basin, we follow the parameter suggestions by Roten et al. (2012) and Table 8.12 of Darendeli (2001), where $\phi_{1-4} = 3.52 \cdot 10^{-2} \pm 9.99 \cdot 10^{-7}$, $1.01 \cdot 10^{-3} \pm 4.16 \cdot 10^{-9}$, $3.25 \cdot 10^{-1} \pm 2.85 \cdot 10^{-3}$, and $3.48 \cdot 10^{-1} \pm 2.20 \cdot 10^{-4}$, respectively, while h_{gw} is set to 3 m and $OCR = 1$. PI is set to 40% for $Vs30 < 300\, m/s$, 30% for $300\, m/s < Vs30 < 450\, m/s$, and 0% for $Vs30 > 450\, m/s$.

The modulus reduction curve is described as in Darendeli (2001)

$$\frac{G}{G_{max}} = \frac{1}{1 + \gamma_{xy}/\gamma_r} \quad , \tag{S7}$$

which builds a relation between the shear modulus ratio to the unloaded maximum strength G/G_{max} and shear strain γ_{xy}, controlled by the reference strain γ_r, and $G/G_{max} = 0.5$ when $\gamma_{xy} = \gamma_r$. The standard deviation σ of G/G_{max} is estimated in Roten et al. (2023) as

$$\sigma\left[\frac{G}{G_{max}}\right] = exp(\phi_{13}) + \sqrt{\frac{0.25}{exp(\phi_{14})}} = 0.09638 \quad , \tag{S8}$$

where $\phi_{13} = -4.23$ and $\phi_{14} = 3.62$ are parameters from Equation (7.29) and Table 8.12 in Darendeli (2001). Thus, the upper and lower limits of the reference strain from around the mean ($\gamma_{r,mean}$) to one standard deviation ($\pm 1\sigma$) can be found by solving Eq. (S7) for the shear strain γ_{xy} when

$$\frac{G}{G_{max}} \pm \sigma = \frac{1}{1 + \gamma_{xy}/\gamma_r} \pm \sigma = 0.5 \quad , \tag{S9}$$

resulting in

$$\gamma_r[\pm 1\sigma] \in (\gamma_{r,mean}/1.478,\ \gamma_{r,mean} \cdot 1.478) \quad . \tag{S10}$$

Similarly, for extreme cases within $\pm 2\sigma$ and $\pm 3\sigma$,

$$\gamma_r[\pm 2\sigma] \in (\gamma_{r,mean}/2.2548,\ \gamma_{r,mean} \cdot 2.2548) \quad , \tag{S11}$$

and

$$\gamma_r[\pm 3\sigma] \in (\gamma_{r,mean}/3.7425,\ \gamma_{r,mean} \cdot 3.7425) \quad , \tag{S12}$$

respectively. In our analysis, we calibrated the soil nonlinear effects by multiplying the scaling factors from Eqs. (S10) to (S12) onto the depth-dependent reference strain model across the nonlinear simulation domain (Figs. 11 to 13).

RESOLUTION OF NONLINEAR SIMULATIONS

Due to the reduction of shear moduli caused by soil nonlinearity and hysteretic behavior, as described in Eq. (S7), the mesh grid resolution required to maintain the same level of accuracy can vary from the linear regime to the Iwan nonlinear model. Fig. S9(a) shows the minimum ratio of the shear modulus at the end of the nonlinear simulation with the Darendeli's reference strain-depth relations minus two standard deviations (G), relative to the undamped shear modulus (G/G_{max}). The shear modulus is reduced to about 1/10 of its undamped value in parts of the model region, with values as low as 0.09 at LKC and 0.4 at other stations (see Fig. S9(b)), corresponding to a minimum V_s of about 43 m/s, which requires a grid spacing of Δh = 0.85 m to maintain 5 points per minimum wave length.

To test whether our mesh accurately resolves the nonlinear damping at these sites, we conducted sensitivity tests at LKC where the largest PGA for the Magna mainshock was recorded and the largest modulus reduction is found. To save computational cost we carried out the tests in two dimensions, in a model 5 km along east-west from the surface to a depth of 2.3 km, using the synthetics from the 3D linear simulation at a depth of 1 km as input. We ensured that the 2D approximation is reasonable through comparison with the 3D model in the linear regime (Fig. S10). Fig. S11 shows Fourier spectra from nonlinear simulations (7 yield surfaces) and the optimal reference strain model (i.e. Darendeli's (2001) -2σ) in this 2D model using Δh = 2.5 m and Δh = 0.85 m. The mean spectral difference between the synthetics with two grid spacings is 0.03 in log_{10} scale (i.e. $\sim 7\%$ in linear scale), suggesting that the 3D simulations accurately resolve the nonlinear damping.

CALCULATION OF SOIL-ROCK SPECTRAL RATIOS

The concept of soil-rock spectral ratios is based on the frequency-domain model of ground motion

$$R_i(r_i, f) = E(f) S_i(r_i, f) D_i(r_i, f) \quad , \tag{S13}$$

where R_i is the ground motion spectral amplitude recorded at station i, and E, S_i, and D_i are the source term, site amplification factor, and distance dependent term, respectively, while r_i is the distance to the source. For a reference rock station (suffix ref) with no site amplification ($S_{ref} = 1$), which is reasonably close to the soil station i and thus has a similar distance term D_i and source effects E, the soil amplification at site i can be approximated from Eq. (S13)

$$S_i(r_i, f) \approx \frac{R_i(r_i, f)}{R_{ref}(r_{ref}, f)} \quad . \tag{S14}$$

For each event, either synthetics or observations, average horizontal Fourier spectra are used as $R_i(r_i, f)$ (soil station) and $R_{ref}(r_{ref}, f)$ (reference rock station) (Pankow and Pechmann, 2004) as

$$\frac{R_i(r_i, f)}{R_{ref}(r_{ref}, f)} = \frac{R_{i,1}(f) + R_{i,2}(f)}{R_{ref,1}(f) + R_{ref,2}(f)} \quad , \tag{S15}$$

where 1 and 2 represent 2 horizontal ground motion components. We generally follow Pankow and Pechmann (2004) in the window selection and windowing of the time series prior to the calculation of the Fourier spectra $R(f)$, applying a 15-sec data window starting 1.5 s before the S-wave arrival, a 10% Hanning taper at both ends of the time series, and a band-pass filter between 0.1 and 10 Hz.

FILTER PARAMETERS

For all simulations and recordings used in this study, we used a 2nd-order Butterworth filter with 2 forward passes.

REFERENCES

Brune, J. N., 1970. Tectonic stress and the spectra of seismic shear waves from earthquakes. *Journal of Geophysical Research (1896-1977)* **75**, 4997–5009. doi:10.1029/JB075i026p04997.

Darendeli, M. B., 2001. Development of a New Family of Normalized Modulus Reduction and Material Damping Curves. Ph.D. thesis, The University of Texas at Austin.

Ely, G., Jordan, T., Small, P., and Maechling, P., 2010. A Vs30-derived Near-surface Seismic Velocity Model. In *AGU Fall Meeting Abstracts*, vol. 2010, pp. S51A–1907.

Nie, S., Wang, Y., Olsen, K. B., and Day, S. M., 2017. Fourth-order staggered-grid finite-difference seismic wavefield estimation using a discontinuous mesh interface (WEDMI). *Bulletin of the Seismological Society of America* **107**, 2183–2193.

Pankow, K. L. and Pechmann, J. C., 2004. *Determination of Low-Strain Site-Amplification Factors in the Salt Lake Valley, Utah, Using ANSS Data*. University of Utah Seismograph Stations.

Roten, D., Olsen, K. B., and Pechmann, J. C., 2012. 3D Simulations of M 7 Earthquakes on the Wasatch Fault, Utah, Part II: Broadband (0–10 Hz) Ground Motions and Nonlinear Soil Behavior. *Bulletin of the Seismological Society of America* **102**, 2008–2030. doi:10.1785/0120110286.

Roten, D., Yeh, T., Olsen, K. B., Day, S. M., and Cui, Y., 2023. Implementation of Iwan-Type Nonlinear Rheology in a 3D High-Order Staggered-Grid Finite-Difference Method. *Bulletin of the Seismological Society of America* **N/A**, N/A. doi:10.1785/0120230011.

114 SUPPLEMENTARY FIGURES

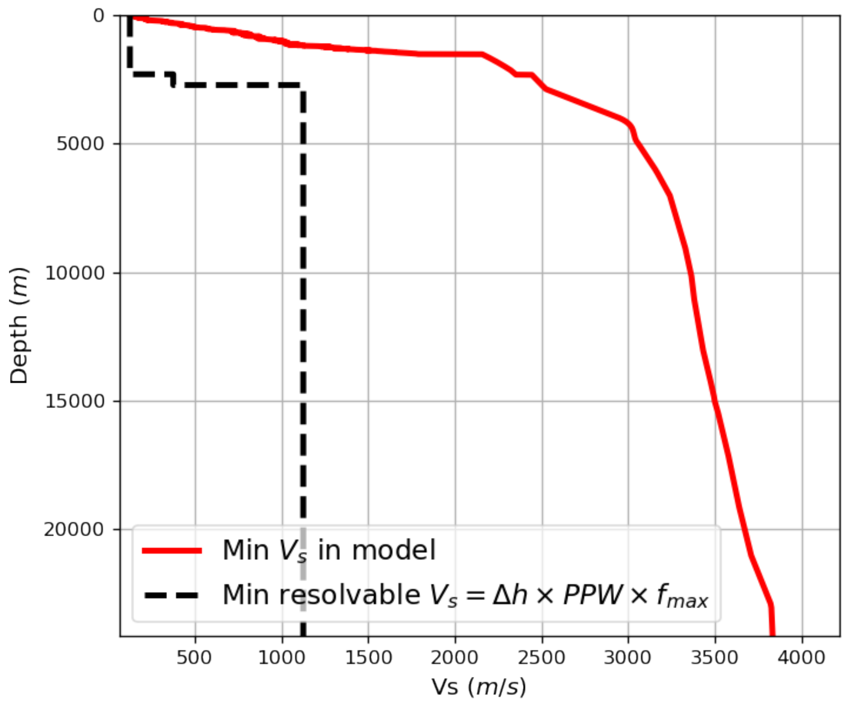

Figure S1. Illustration of the resolution of the velocity model along depth using a 3-block discontinuous mesh, showing that the minimum V_s in the CVM is sampled by at least 5 points per minimum V_s wavelength (PPW).

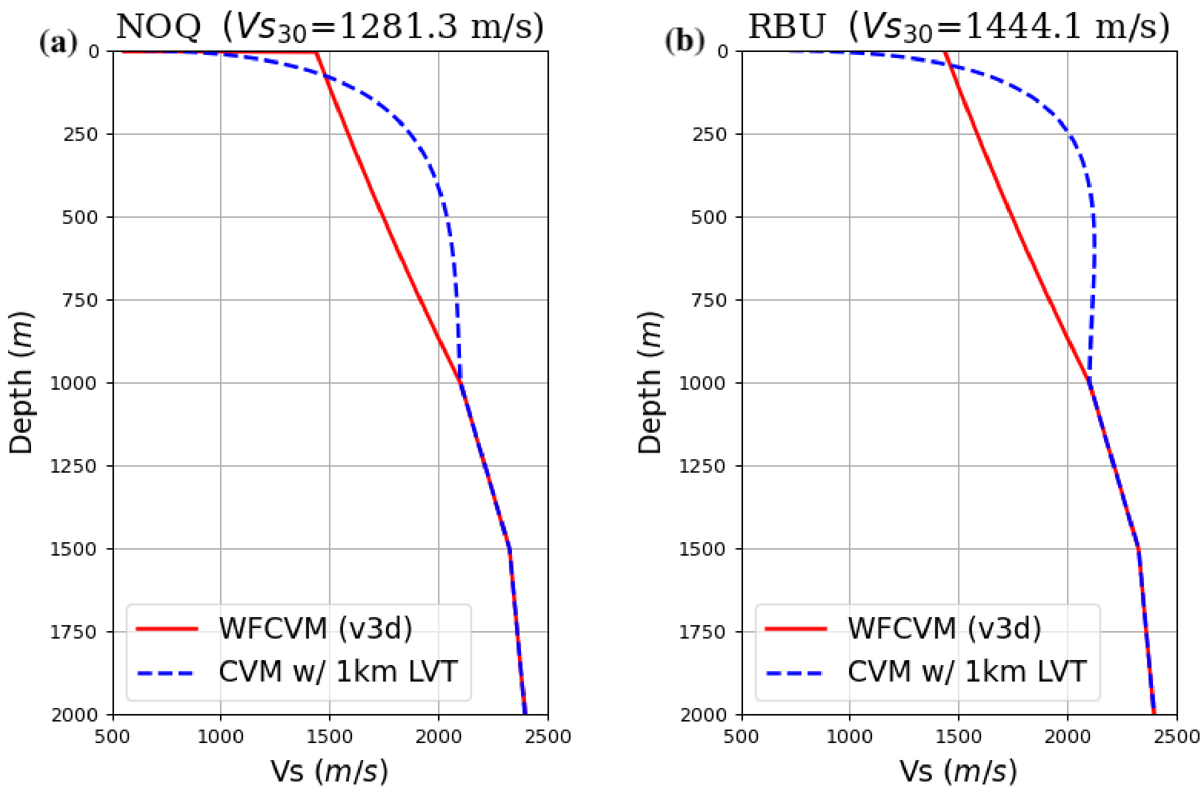

Figure S2. V_s profiles with LVT at rock stations (a) NOQ, and (b) RBU, using a 1,000 m tapering depth following Eq. (S4) and Ely et al. (2010). See Fig. 1(b) for station locations.

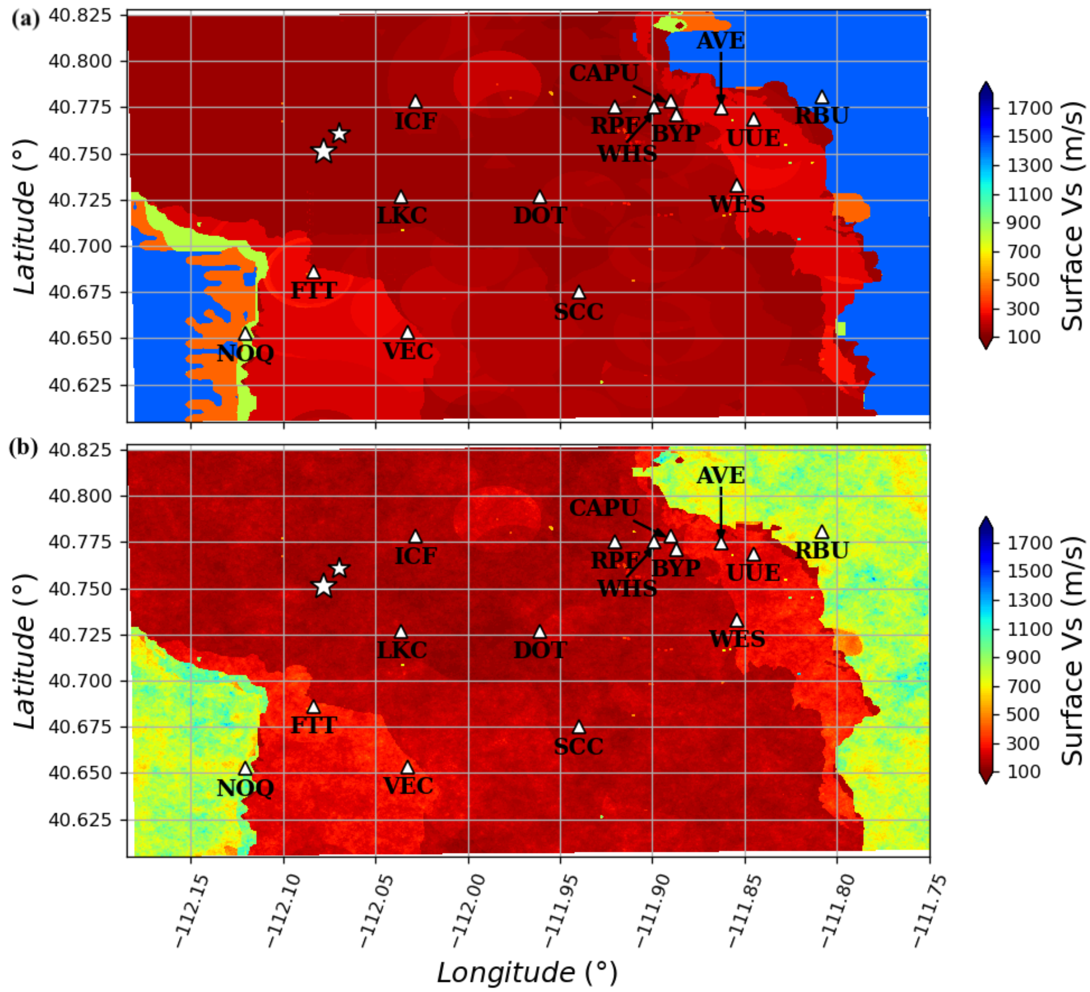

Figure S3. Surface V_s across the modeling region (see white rectangle in Fig. 1(b)). (a) before and (b) after adding the LVT and SSHs to the WFCVM. The stars depict the epicenters of the 2020 Magna mainshock and the M_w4.59 aftershock, and the triangles are seismic stations.

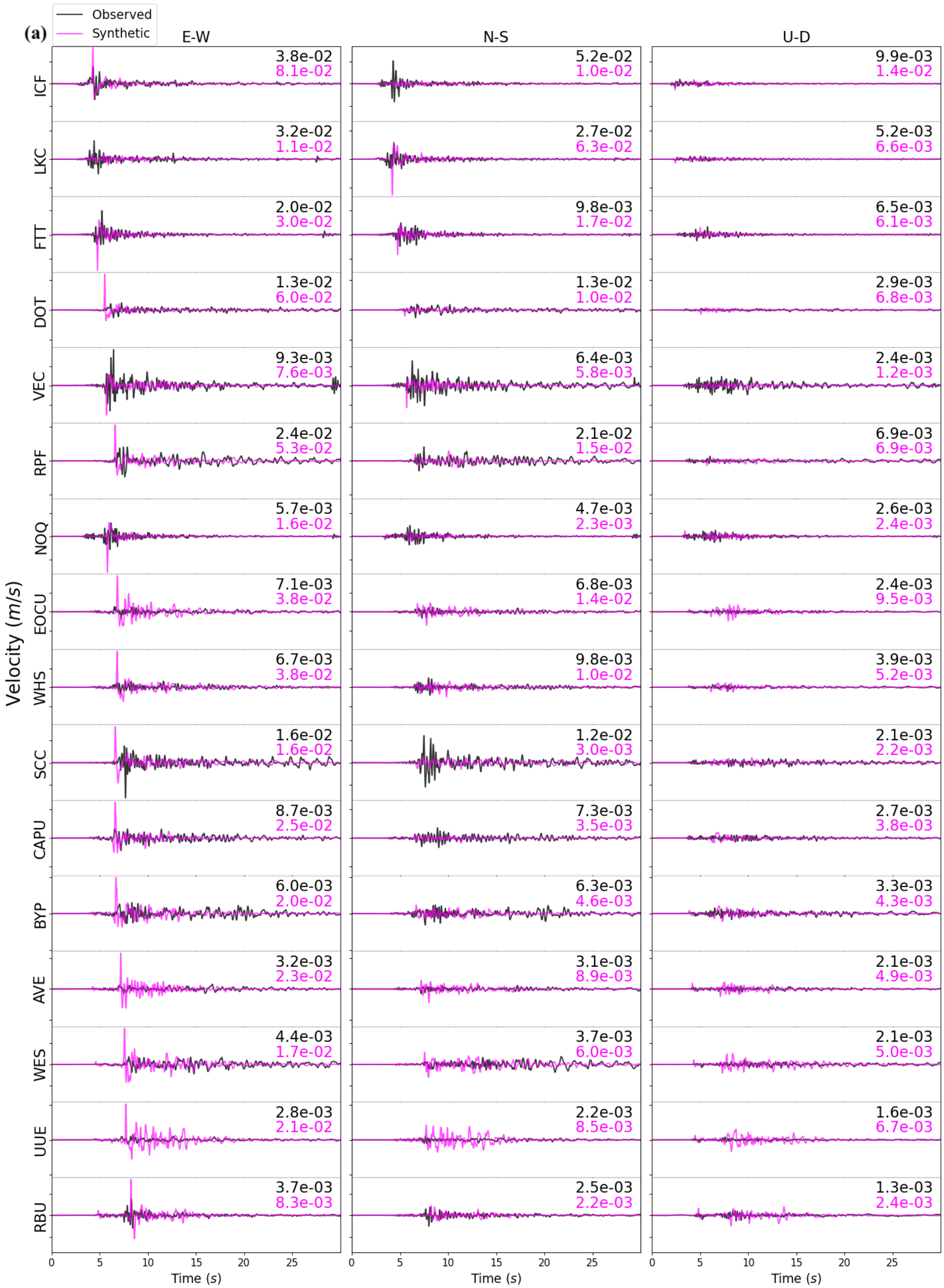

Figure S4. *(see next page)*

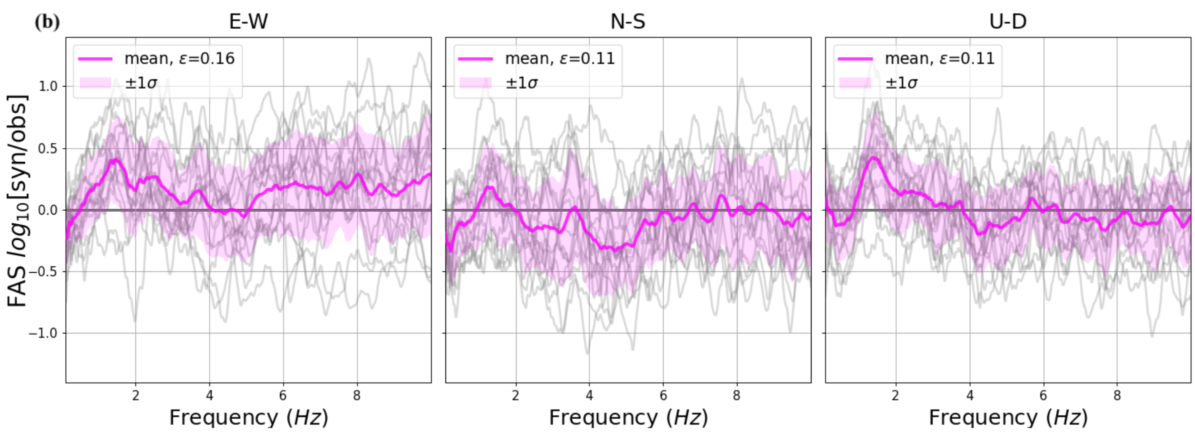

Figure S4 ***(previous pages)*****.** Comparison of 0.1-10 Hz synthetics from our optimal model and observations for the M_w4.59 aftershock. (a) Velocity time series, with peak values for both synthetics and observations listed in m/s, and (b) Fourier acceleration spectral bias, with ε depicting mean error over all stations. See Fig. 1(b) for station locations.

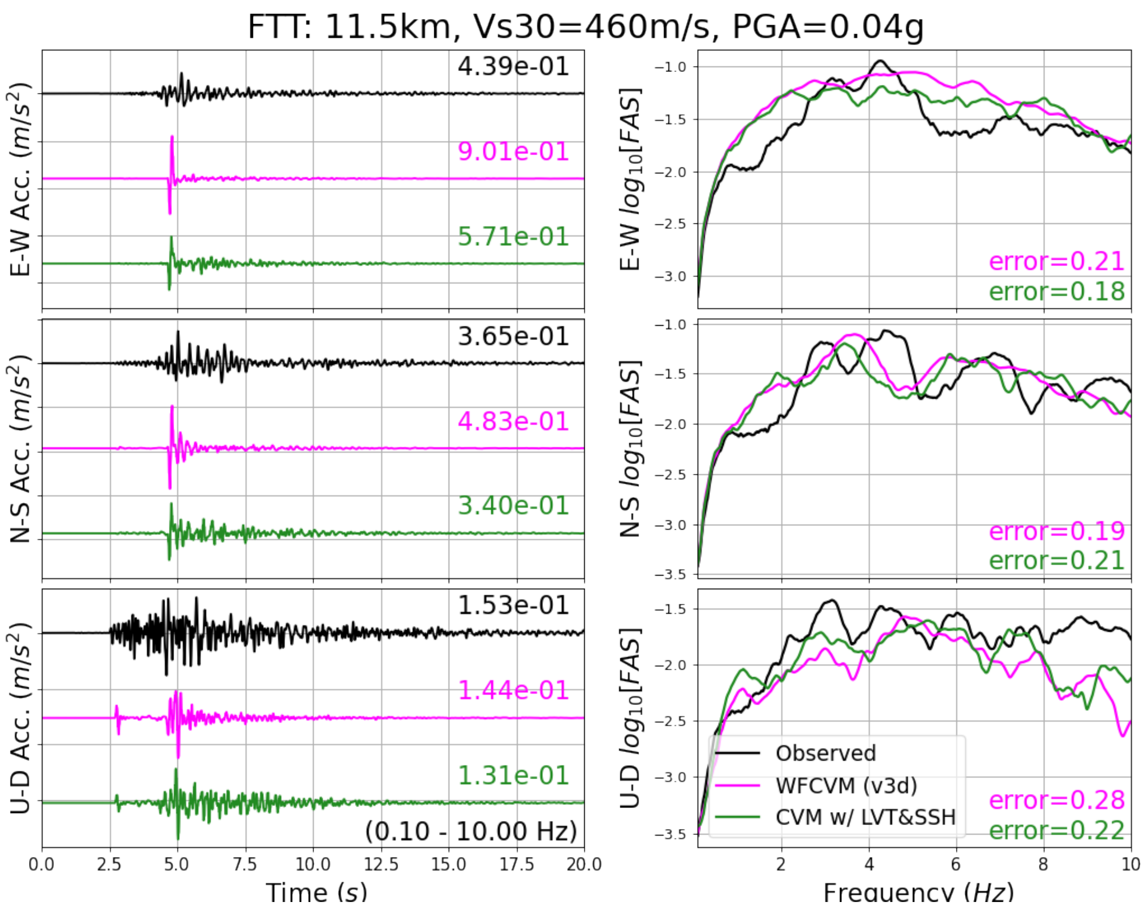

Figure S5. Comparison of synthetic (colored) and observed (black) acceleration time series (left panels) and Fourier acceleration spectra (right panels) for the M_w4.59 aftershock at station FTT. Both sets of synthetics are calculated in the WFCVM using the optimal Q model of $Q_S = 0.05 V_S f^{0.4}$ (Eq. (1)). Additionally, the green time series include the effects of the LVT outside the basin (see Eq. (S4) and Fig. 1(b)), as well as the optimal SSH with vertical and horizontal correlation lengths of 400 m and 2,000 m, respectively, Hurst number of 0.05 and 10% standard deviation. Both data and synthetics are band-pass filtered between 0.1 and 10.0 Hz. Peak acceleration values are listed in m/s^2 by the waveforms, and the average absolute FAS errors in log scale are listed below the spectra. For station locations, see Fig. 1(b).

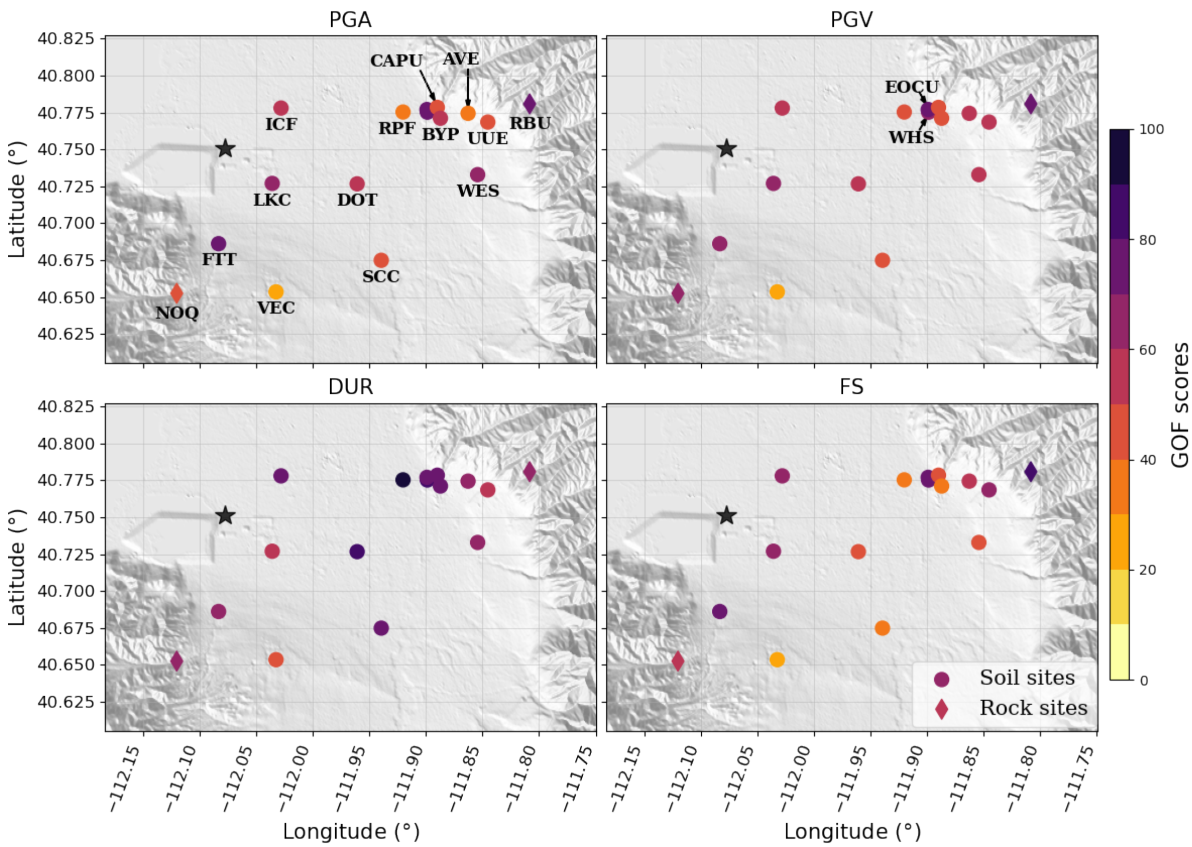

Figure S6. GOF maps for 0.1-1.0 Hz PGA, PGV, DUR, and FS from our optimal linear simulation of the M_w5.5 main shock. The epicenter is denoted by the star.

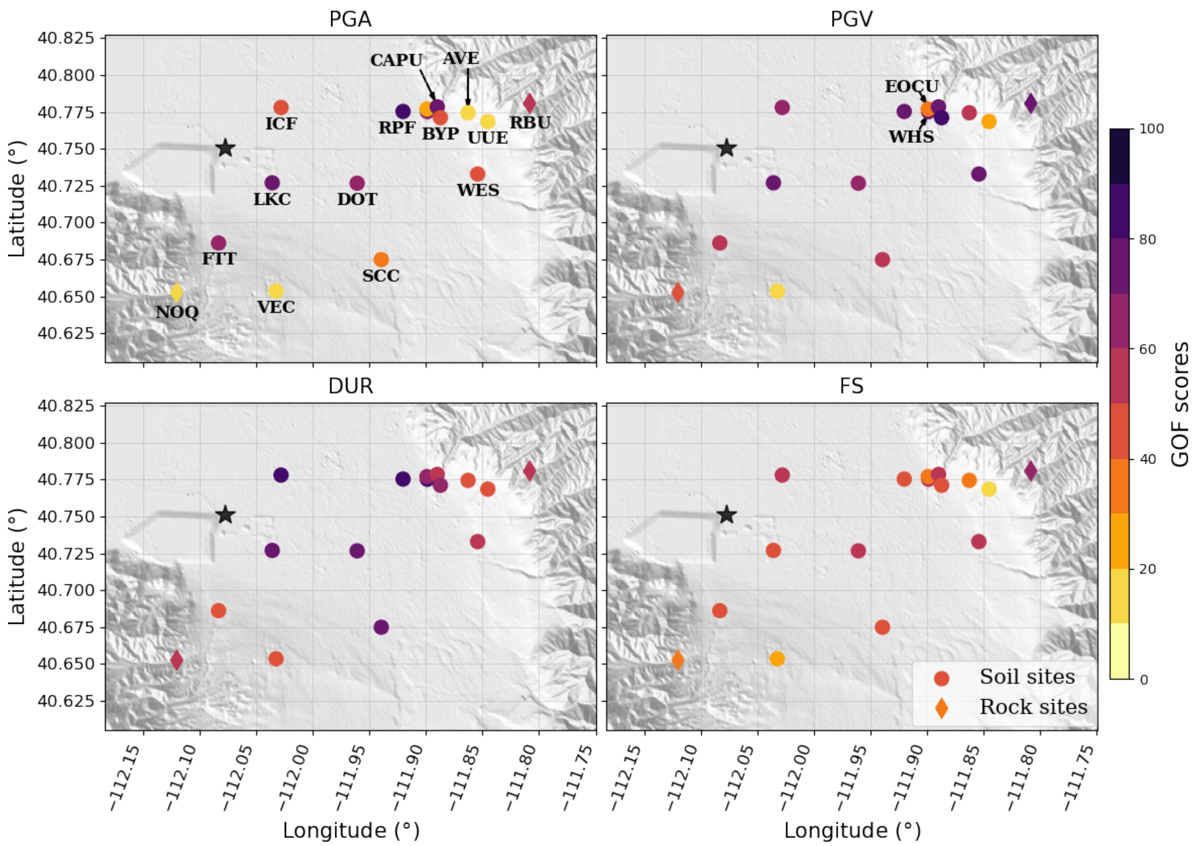

Figure S7. Same as Fig. S6, but for synthetics and data band-pass filtered between 0.1-10.0 Hz.

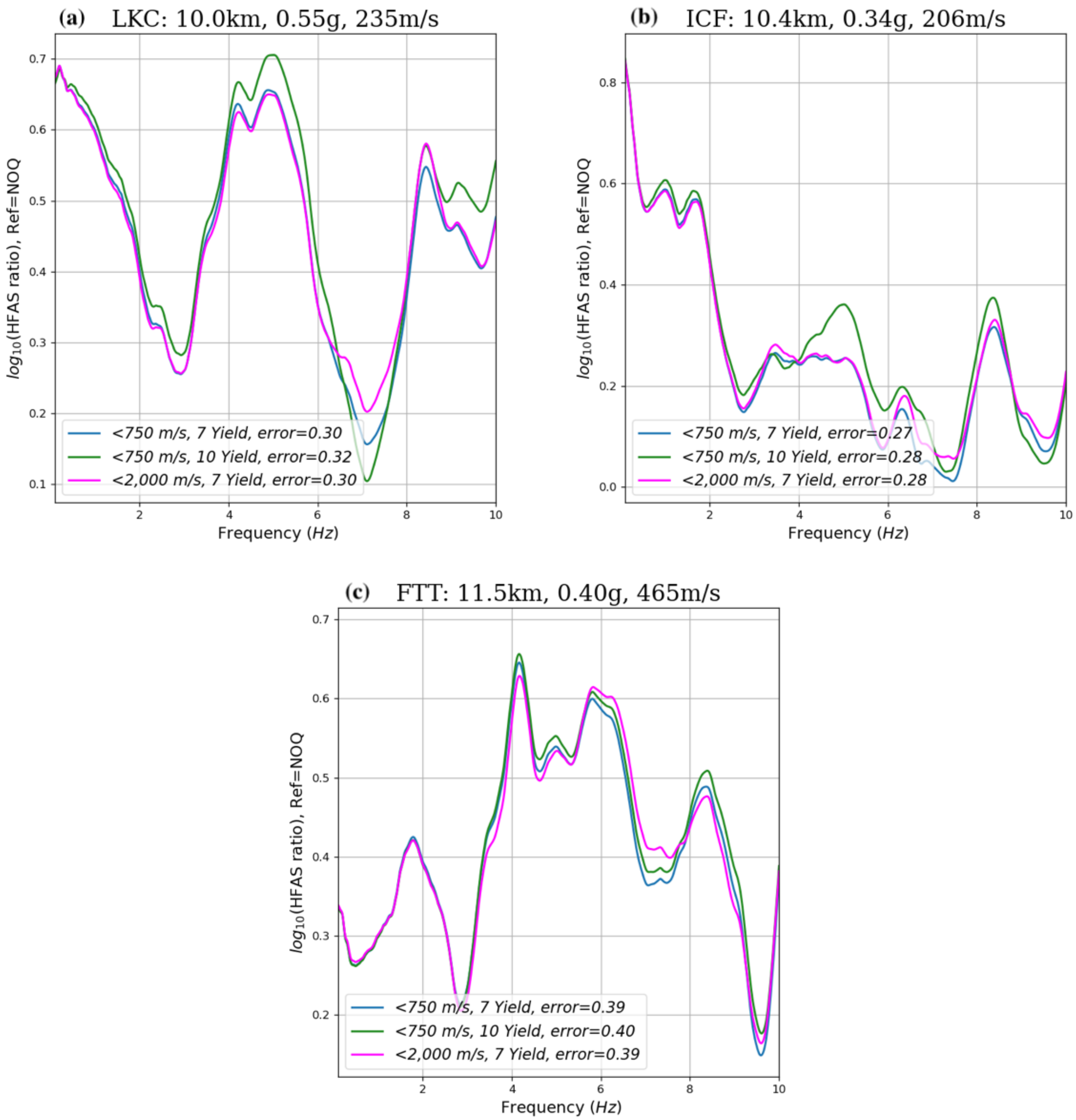

Figure S8. Comparison of synthetic and observed horizontal spectral amplification ratios for the Magna main shock at stations (a) LKC, (b) ICF and (c) FTT, using NOQ as reference. Results are shown for nonlinear simulations with the mean values of Darendeli's (2001) reference strain-depth relation, applied for $V_s < 750$ m/s, using 7 and 10 yield surfaces (green and blue spectra, respectively), as well as for V_s <2,000 m/s and 7 yield surfaces (magenta curve). See Fig. 1(b) for station locations.

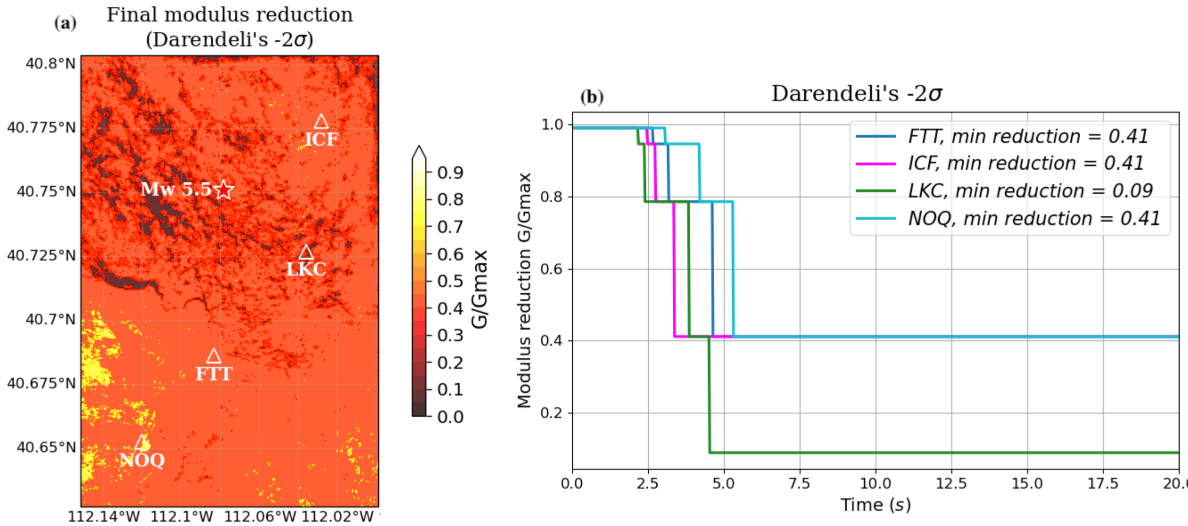

Figure S9. Shear modulus reduction G/G_{max} during the 3D nonlinear simulations for the Magna main shock (i.e., the ratio between the nonlinearly reduced and the linear shear modulus), using Darendeli's -2σ reference strain relation. (a) Distribution of final modulus reduction in this simulation domain, showing the minimum G/G_{max} ratio during the simulation. (b) Minimum shear modulus reduction ratios during the nonlinear simulation at FTT, ICF, LKC and NOQ.

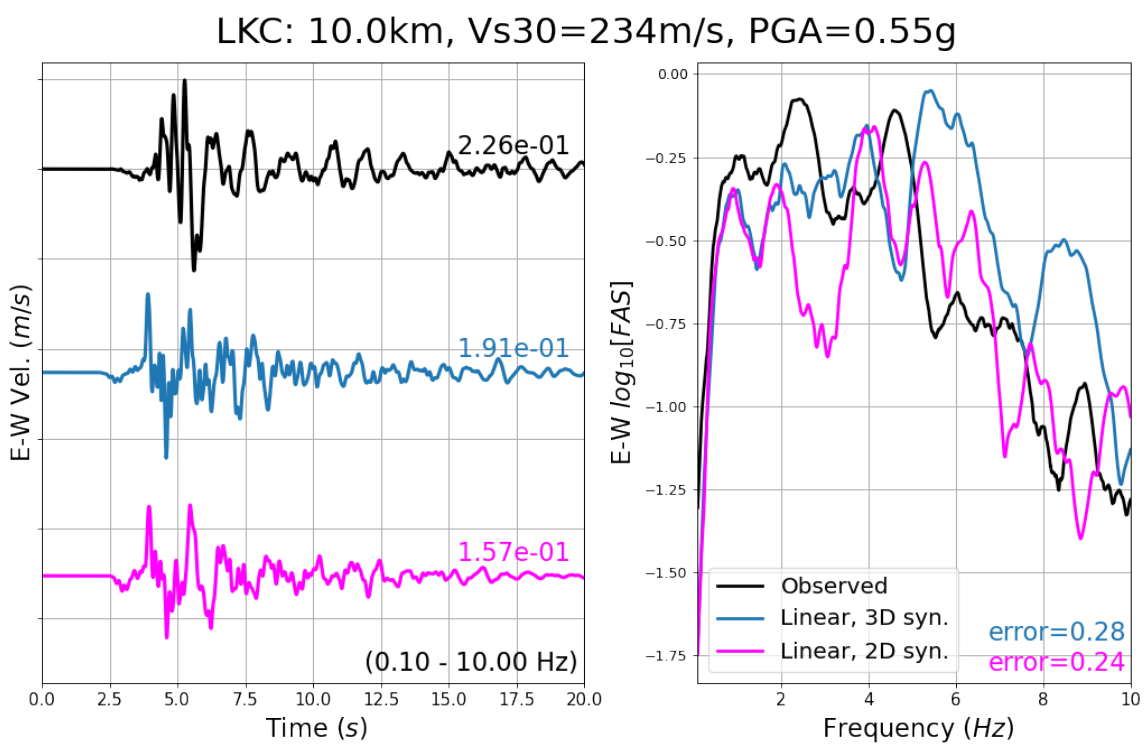

Figure S10. Comparison of synthetic and observed (left) velocity time series and (right) Fourier acceleration spectra at LKC along the E-W component. Blue curves are from the 3D simulation, while magenta curves are from the 2-step simulations, with the 2D simulation using synthetics from the 3D linear simulation at a depth of 1 km as a plane wave source. See Fig. 1(b) for the station location.

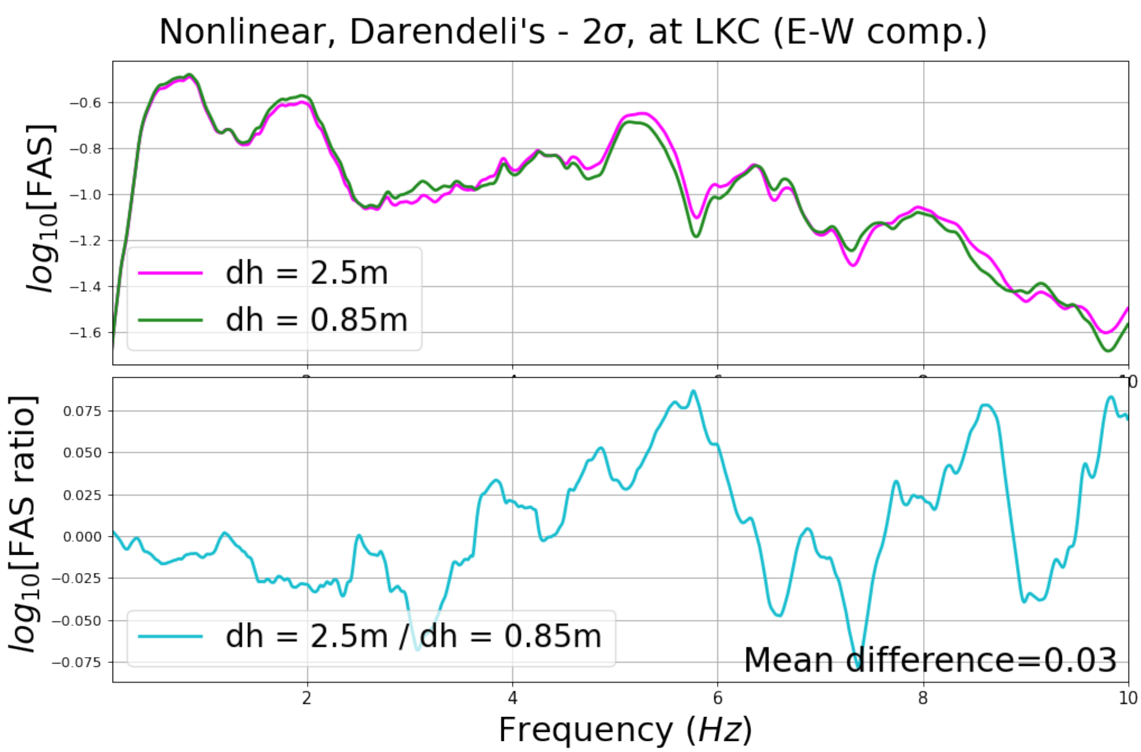

Figure S11. Comparison of 2D synthetic (top) Fourier acceleration spectra at LKC for Δh = 2.5 m and Δh = 0.85 m, and (bottom) the spectral ratio between the spectra, in units of log_{10}.